

Convection by a horizontal thermal gradient

H. J. J. GRAMBERG, P. D. HOWELL AND J. R. OCKENDON

OCIAM, Mathematical Institute, University of Oxford, Oxford OX1 3LB, UK

(Received 12 May 2006 and in revised form 13 March 2007)

This paper considers a paradigm large-Prandtl-number, large-Rayleigh-number forced convection problem suggested by the batch melting process in the glass industry. Although the fluid is heated from above, non-uniform heating in the horizontal direction induces thermal boundary layers in which colder liquid is driven over hotter liquid. This leads to an interesting selection problem in the boundary layer analysis, whose resolution is suggested by a combination of analytical and numerical evidence.

1. Introduction

This paper concerns the structure of slow two-dimensional convective flow in a rectangular container whose horizontal upper boundary is subject to a prescribed temperature gradient. In steady flow, the vertical temperature profile varies from one of stable stratification to one of unstable stratification as we move down the temperature gradient at the upper boundary, and a circulation is set up in which the liquid near the top moves down this temperature gradient.

Our work is motivated by the study of batch melting in the glass industry, in which a solid granular material usually consisting mostly of sand is fed into a glass-melting tank as in figure 1. In a so-called ‘bridge-wall’ furnace, steady radiative heating is applied to the top of the tank, and the batch melts at both the top and the bottom of the ‘blanket’, which is the wedge-shaped region shown in figure 1. Since the average density of the blanket is lower than the density of the molten glass, there is little molten glass on the top of the batch, which floats above the melt but only partially covers the melt surface. The melt is removed for further processing at the downstream end of the tank. Since the batch blanket works as an insulator for radiative heating, the temperature is greater at the surface of the uncovered glass than directly beneath the batch. Due to buoyancy, this temperature difference forces a convective flow of hot glass under the batch towards the feed point, and this influences the melting and length of the blanket.

In this paper, we will study a prototype for such convective flows that are driven by horizontally non-uniform heating from above. We will avoid the complication of modelling the batch blanket by assuming instead that the top surface of the glass is free of stress and at a prescribed temperature which is an increasing function of x . We will also ignore other important real-world effects by assuming that the flow is two-dimensional, that the viscosity and the thermal conductivity are constant, and that the Boussinesq approximation is valid. Even with these simplifications, our model poses many interesting mathematical challenges, both analytically and numerically.

A lot of research has been done on convection due to a horizontal temperature gradient in a rectangular cavity. Most of this work concerns cavities whose vertical walls are kept at different temperatures. In Batchelor (1954), Elder (1965) and Gill (1966), for example, this problem has been investigated in the case where the aspect

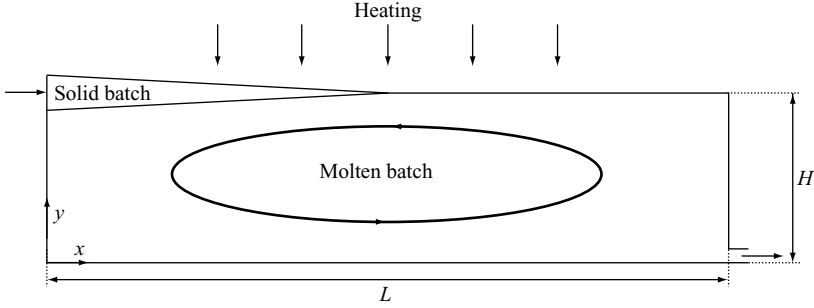


FIGURE 1. Schematic overview of the bath. The length of the bath is L and the height is H .

ratio H/L is very large. Batchelor (1954) considered cases where the Rayleigh number Ra is either very small or very large. In the latter case, Batchelor predicted a flow with thin thermal boundary layers along the solid walls of the cavity and an isothermal core. After the experimental work done by Elder (1965), Gill (1966) modified the model when $Ra \gg 1$ by assuming that the temperature in the core is only a function of the vertical coordinate. Small aspect ratio baths were investigated by Daniels (1993) and Cormack *et al.* (1974), who found that the flow consists of a core region where the streamlines are more or less horizontal and the temperature is approximately linear in the horizontal coordinate and independent of the vertical coordinate, and the regions near the ends of the bath where the flow turns through 180° . Daniels (1993) showed that for $Ra \gg 1$, the thickness of these latter regions is proportional to $(RaH/L)^{-3/5}$.

However, as far as the present authors are aware, very little research has been done on the case where horizontal temperature gradients are caused by keeping the vertical walls insulated and prescribing the temperature at the top surface of the bath.

2. The mathematical model

In our paradigm model, the velocity $\mathbf{u} = (u, v)$, the excess pressure p (with the hydrostatic pressure subtracted), and the temperature T measured relative to the coldest surface temperature at the top left-hand corner of the bath satisfy the equations of conservation of mass, momentum, and energy in the form

$$\nabla \cdot \mathbf{u} = 0, \quad (2.1)$$

$$(\mathbf{u} \cdot \nabla) \mathbf{u} = -\frac{1}{\rho} \nabla p + \nu \nabla^2 \mathbf{u} + \mathbf{g}, \quad (2.2)$$

$$\mathbf{u} \cdot \nabla T = \kappa \nabla^2 T. \quad (2.3)$$

Here ρ , ν , and κ are the constant density, kinematic viscosity, and thermal diffusivity, and $\mathbf{g} = (0, \alpha g T)$ where α is the thermal expansion coefficient and g is the gravitational acceleration. Note that in (2.3), we neglect dissipation. The bath occupies the region $0 < x < L$, $0 < y < H$.

We work with physical parameters typical for glass in batch melting for which (see Krause & Loch 2002, p. 105)

$$\rho \sim 2 \times 10^3 \text{ kg m}^{-3}, \quad \kappa \sim 10^{-5} \text{ m}^2 \text{ s}^{-1}, \quad \nu \sim 10^{-2} \text{ m}^2 \text{ s}^{-1}, \quad \alpha \sim 10^{-5} \text{ K}^{-1}. \quad (2.4)$$

Also, for a typical furnace, the height $H \sim 1$ m, the length $L \sim 10$ m, and the surface temperature varies by $\Delta T \sim 600\text{K}$. Hence, when we non-dimensionalize T with ΔT ,

p with $\rho g \alpha H \Delta T$, x, y with H and \mathbf{u} with $U \kappa \sqrt{Ra}/H$, we are led to the dimensionless model

$$\nabla \cdot \mathbf{u} = 0, \quad (2.5)$$

$$\frac{U^2}{Pr} (\mathbf{u} \cdot \nabla) \mathbf{u} = -\nabla p + \frac{U}{\sqrt{Ra}} \nabla^2 \mathbf{u} + T \mathbf{j}, \quad (2.6)$$

$$\sqrt{Ra} U (\mathbf{u} \cdot \nabla) T = \nabla^2 T. \quad (2.7)$$

Here, $Pr = \nu/\kappa \sim 10^3$ is the Prandtl number and $Ra = \alpha g \Delta T H^3/\nu \kappa \sim 10^4$ is the Rayleigh number, while U is a dimensionless velocity scale which, crucially, is yet to be determined. Indeed, one of our principal aims is to predict the magnitude of the fluid velocity. For the moment, we note that a velocity of around $3 \times 10^{-3} \text{ mm s}^{-1}$ is typically observed in a glass furnace, and this corresponds to $U \approx 1$.

On the sides and the base of the bath, we impose zero slip and insulating boundary conditions, i.e.

$$\mathbf{u} = \mathbf{0}, \quad \frac{\partial T}{\partial n} = 0, \quad \text{on } y=0, \quad x=0, \quad \text{and } x=\delta^{-1}, \quad (2.8)$$

where δ is the aspect ratio H/L . On the upper boundary, in reality there is a radiative heat flux from above into the free surface and a lower heat flux into the region covered by the batch. In addition, the free surface is subject to zero traction, while the fluid adjacent to the batch effectively satisfies zero slip conditions. Our aim in the first instance is to understand the bulk convective flow induced by the horizontal thermal gradient so, instead, we suppose that the surface temperature is a known function $T_0(x)$, with $T'_0 > 0$. For the velocity, we impose zero stress conditions over the entire surface.

By introducing a stream function ψ , where $u = \partial\psi/\partial y$ and $v = -\partial\psi/\partial x$, we automatically satisfy (2.5). After elimination of the pressure from (2.6), we get

$$\frac{U^2}{Pr} \frac{\partial (\nabla^2 \psi, \psi)}{\partial (x, y)} = \frac{U}{\sqrt{Ra}} \nabla^4 \psi - \frac{\partial T}{\partial x}, \quad (2.9)$$

$$\sqrt{Ra} U \frac{\partial (T, \psi)}{\partial (x, y)} = \nabla^2 T, \quad (2.10)$$

and the boundary conditions are

$$\psi = \frac{\partial \psi}{\partial x} = \frac{\partial T}{\partial x} = 0 \quad \text{on } x=0 \text{ and } x=\delta^{-1}, \quad (2.11)$$

$$\psi = \frac{\partial \psi}{\partial y} = \frac{\partial T}{\partial y} = 0 \quad \text{on } y=0, \quad (2.12)$$

$$\psi = \frac{\partial^2 \psi}{\partial y^2} = 0, \quad T = T_0(x) \quad \text{on } y=1. \quad (2.13)$$

Before proceeding further, we note that integration of (2.10) over the bath and application of the boundary conditions (2.11)–(2.13) leads to the identity

$$\int_0^{\delta^{-1}} \frac{\partial T}{\partial y}(x, 1) dx = 0. \quad (2.14)$$

This represents global conservation of energy, stating that there can be no net heat flow across the top of the bath.

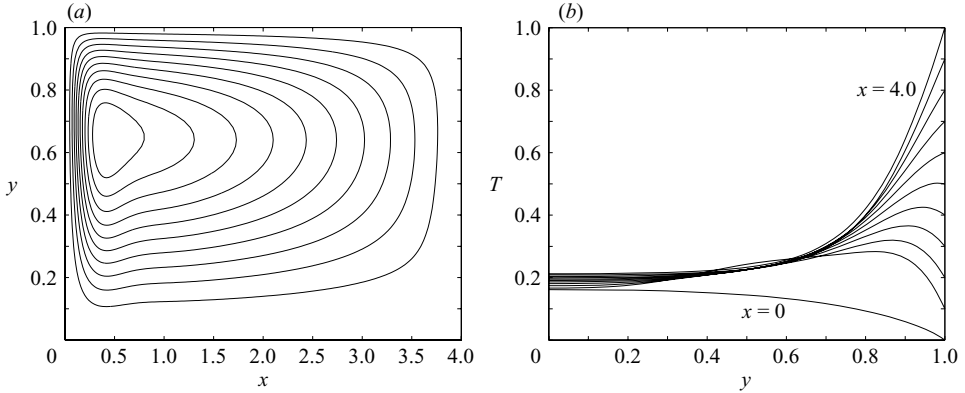


FIGURE 2. (a) Streamlines and (b) T as a function of y for $x=0, 0.4, \dots, 4.0$ in the case where $\delta=0.25$, $Ra=1.6 \times 10^5$ (corresponding to $\varepsilon=0.1$), and $Pr=10^2$.

In view of our uncertainty about U , we will begin by discussing numerical solutions in §3. Since $Ra \gg 1$, we expect boundary layers to occur, and we will analyse these in §4. However, the numerical evidence will provide us with vital clues as to the structure of the solution and our decision about U .

3. Numerical results

We have calculated the temperature and velocity field using FEMLAB, where we used the dimensional model (2.1)–(2.3), and afterwards scaled the numerical results for the temperature and velocity with ΔT and $\kappa\sqrt{Ra}/H$, respectively, which is equivalent to setting $U=1$. For the temperature profile at $y=1$ and the aspect ratio, we have taken $T_0=\delta x$ and $\delta=0.25$. In figure 2(a), we plot the streamlines for the ‘low viscosity’ flow $Ra=1.6 \times 10^5$, and $Pr=10^2$, which corresponds to $\varepsilon=0.1$, where $\varepsilon=1/\sqrt{\delta\sqrt{Ra}}$ is a parameter that will be important. They suggest the appearance of a downward boundary layer near $x=0$ and a horizontal layer near $y=1$. The thicknesses of these boundary layers appear to be of approximately the same order.

In figure 2(b), we plot the temperature as a function of y for several values of x . For $0 < y < 0.7$ and $\delta x > 0.1$, the temperature is around 0.2, but near $y=1$, $\partial T/\partial y$ becomes large, which also suggests that there is a thermal boundary layer near $y=1$. The boundary layer behaviours near $y=1$ and $x=0$ become more pronounced when we increase Ra to 2×10^6 (corresponding to $\varepsilon=0.053$), and Pr to 10^3 , as can be seen in figures 3(a) and 3(b). These pictures suggest that, for increasing Rayleigh numbers, there are thinner boundary layers in the temperature and the velocity field near the top and left walls of the bath.

From (2.4), it follows that for typical parameter values in a glass furnace, $Pr/\delta\sqrt{Ra} \sim 10^2$. Therefore, we suspect that the inertia terms in (2.6) are negligible relative to viscosity and buoyancy. This suspicion is confirmed by figure 4, where we plot the streamlines and temperature distribution in the case where $Ra=1.6 \times 10^5$ and $1/Pr=0$, and by figure 5, where we compare the velocity at the top of the bath in two cases where Pr is large but finite with the case where $1/Pr=0$. From these pictures, we deduce that there is practically no influence of inertia on the velocity and the temperature distribution in the case where $Ra=1.6 \times 10^5$ and $Pr=10^2$. Figure 5 also shows that, for $Ra=2 \times 10^6$, the match between the velocity in the case where inertia is taken into account and the velocity in the case where inertia is neglected

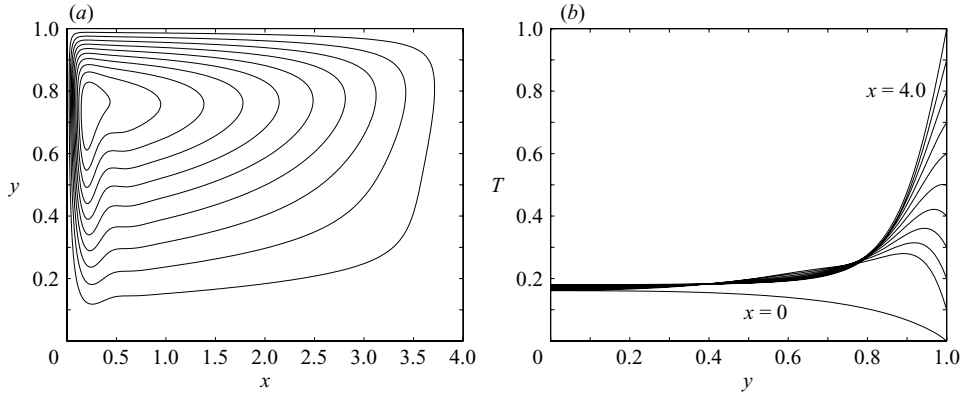


FIGURE 3. (a) Streamlines and (b) T as a function of y for $x=0, 0.4, \dots, 4.0$ in the case where $\delta=0.25$, $Ra=2 \times 10^6$ (or $\varepsilon=0.053$), and $Pr=10^3$.

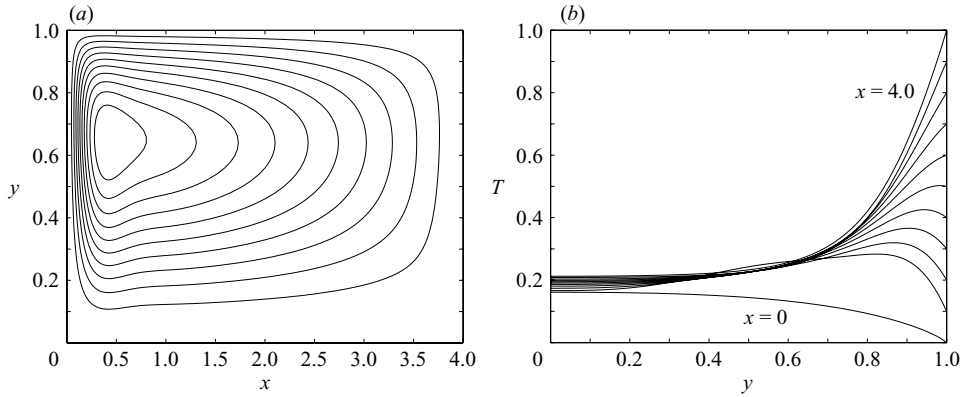


FIGURE 4. (a) Streamlines and (b) T as a function of y for $x=0, 0.4, \dots, 4.0$ in the case where $\delta=0.25$, $Ra=1.6 \times 10^5$ ($\varepsilon=0.1$), and $1/Pr=0$.

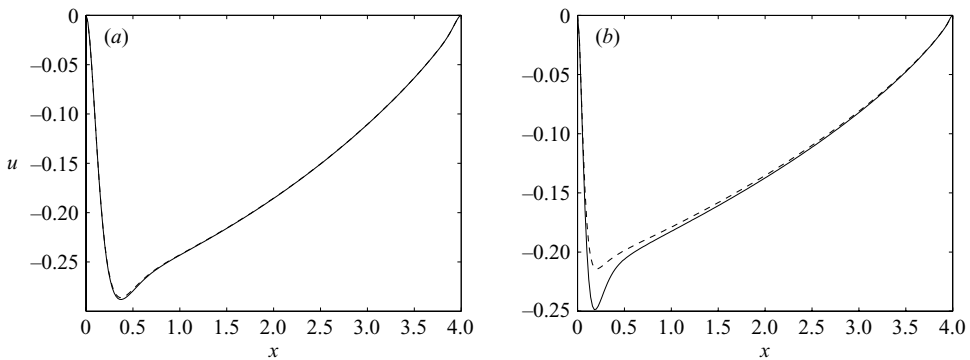


FIGURE 5. The horizontal velocity at the top of the bath in the case where $\delta=0.25$ and (a) $Ra=1.6 \times 10^5$ ($\varepsilon=0.1$) and (b) $Ra=2 \times 10^6$ ($\varepsilon=0.053$). The solid curves are plots of the velocity when $1/Pr=0$ and the dashed curves are when (a) $Pr=10^2$ and (b) $Pr=10^3$.

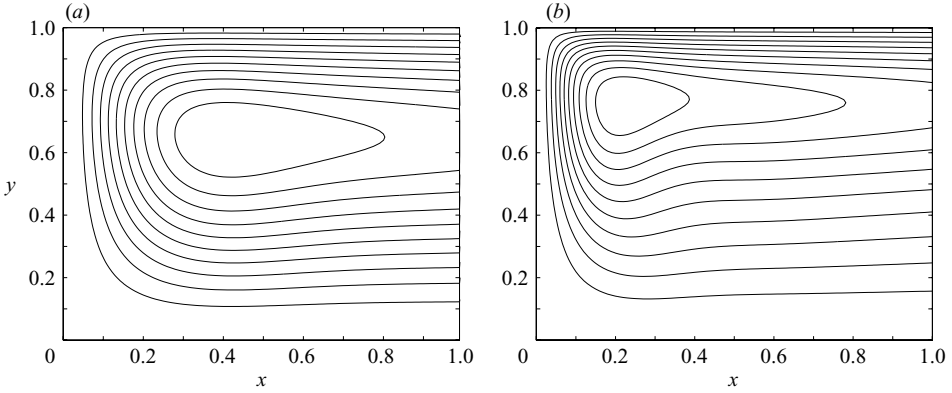


FIGURE 6. Streamlines near the left-hand side of the bath in the case where (a) $Ra = 1.6 \times 10^5$ ($\varepsilon = 0.1$) and $Pr = 10^2$ and (b) $Ra = 2 \times 10^6$ ($\varepsilon = 0.053$) and $Pr = 10^3$.

is quite good, though not as good as in figure 5(a), and outside a boundary layer near $x = 0$ the difference between the solutions is small enough to allow us to neglect inertia in the cases where $Ra = 2 \times 10^6$ and $Pr = 10^3$.

Note that figures 2(a)–3(a), seem to suggest that the streamlines bunch up near the left-hand side of the bath. However, one should realize that the aspect ratio of these figures is δ^{-1} . In figure 6, we have plotted the streamlines for the same values of Ra and Pr , near the left-hand side of the bath such that the aspect ratio of the figures is 1.

Figure 6 shows that the width of the turnover region is of the same order as the height of the bath.

4. Boundary layer analysis

4.1. The outer region

In the light of the earlier discussion, we now let $1/Pr \rightarrow 0$ and look for the asymptotic solution when Ra is large and δ is small, such that $Ra \gg \delta^{-2}$. From (2.10), by an argument analogous to that used in the Prandtl–Batchelor theorem (Batchelor 1956), we expect that T is approximately constant inside any closed streamline. Indeed, assuming that the streamlines are all closed and that $U\sqrt{Ra} \gg 1$, (2.10) tells us that

$$T = T^{(0)}(\psi) + O\left(\frac{1}{U\sqrt{Ra}}\right), \quad (4.1)$$

so that, around any streamline $\psi = c$,

$$0 = \oint_{\psi=c} \frac{\partial T}{\partial n} ds \sim \frac{dT^{(0)}}{d\psi} \oint_{\psi=c} \frac{\partial \psi}{\partial n} ds. \quad (4.2)$$

Since c is arbitrary and $\partial \psi / \partial n < 0$ (the direction of the flow is anticlockwise), we deduce that $T^{(0)} = C_0$ is constant. By repeating this argument successively with

$$T = C_0 + \frac{T^{(1)}(\psi)}{U\sqrt{Ra}} + \dots, \quad (4.3)$$

and so forth, we find that T is a constant C in the outer region with exponential accuracy. The fact that $T = C$ does not satisfy the boundary condition (2.13) indicates the presence of a thermal boundary layer near the top of the bath.

Now considering (2.9) with $1/Pr \rightarrow 0$ and constant T , we find that ψ satisfies the biharmonic equation

$$\nabla^4 \psi = 0. \quad (4.4)$$

The boundary conditions for (4.4) are given by (2.11) and (2.12) on the base and the walls of the bath, while on the top surface we have

$$\psi = 0, \quad \frac{\partial \psi}{\partial y} = u_0(x), \quad \frac{\partial^2 \psi}{\partial y^2} = \omega_0(x) \quad \text{on } y = 1, \quad (4.5)$$

where u_0 and ω_0 are the apparent surface velocity and vorticity seen by the outer solution at the bottom of the boundary layer. Neither of these is known as yet, but they can in principle be related via the Green's function for the biharmonic equation in our rectangular domain.

Our task is vastly simplified if, in addition to the assumptions made so far, we use the smallness of δ to invoke the lubrication approximation. This is formalized by rescaling $x = X/\delta$, so that (4.4) reduces to

$$\frac{\partial^4 \psi}{\partial y^4} = O(\delta^2), \quad (4.6)$$

and the leading-order solution subject to (2.12) and (4.5) is

$$\psi = u_0 y^2 (y - 1). \quad (4.7)$$

It follows that

$$\omega_0 = 4u_0, \quad (4.8)$$

but we emphasize that this result follows from using lubrication theory, and is certainly invalid in the two-dimensional regions near the two ends $X = 0$, $X = 1$.

Now, to determine u_0 , we must examine a coupled thermal/mechanical boundary layer in which the temperature adjusts from the constant value of C to the specified surface profile $T_0(X)$.

4.2. Boundary layer region

Let ε be the unknown boundary layer thickness near $y = 1$. We scale $1 - y$, ψ , and T according to $1 - y = \varepsilon \hat{y}$, $\psi = -\varepsilon \hat{\psi}$, and $T(X, 1 - \varepsilon \hat{y}) = \hat{T}(X, \hat{y})$, which gives us, in a downward-pointing coordinate system,

$$\frac{\partial \hat{T}}{\partial X} = -\frac{U}{\varepsilon^3 \delta \sqrt{Ra}} \frac{\partial^4 \hat{\psi}}{\partial \hat{y}^4}, \quad (4.9)$$

$$\frac{\hat{\psi}}{\hat{y}} \frac{\partial \hat{T}}{\partial X} - \frac{\partial \hat{\psi}}{\partial X} \frac{\partial \hat{T}}{\partial \hat{y}} = \frac{1}{\varepsilon^2 \delta \sqrt{Ra}} \frac{1}{U} \frac{\partial^2 \hat{T}}{\partial \hat{y}^2}, \quad (4.10)$$

with the boundary conditions

$$\hat{\psi} = \frac{\partial^2 \hat{\psi}}{\partial \hat{y}^2} = 0, \quad \hat{T} = T_0 \quad \text{at } \hat{y} = 0, \quad (4.11)$$

and matching conditions

$$\hat{T} \rightarrow C, \quad \frac{\partial \hat{\psi}}{\partial \hat{y}} \rightarrow u_0 \quad \text{as } \hat{y} \rightarrow \infty. \quad (4.12)$$

The important point to note is that the leading-order outer solution $\hat{\psi} \sim u_0 \hat{y}$ satisfies (4.11) identically, implying that the solution takes the form

$$\hat{\psi}(X, \hat{y}) = u_0(X)\hat{y} + \varepsilon \hat{\psi}_1(X, \hat{y}) + \dots \quad (4.13)$$

A balance in (4.9) and (4.10) is now obtained with the scalings

$$\frac{U}{\varepsilon^3 \delta \sqrt{Ra}} = \frac{1}{\varepsilon}, \quad \frac{1}{\varepsilon^2 \delta \sqrt{Ra}} \frac{1}{U} = 1, \quad (4.14)$$

and, hence,

$$U = 1, \quad \varepsilon = (\delta^2 Ra)^{-1/4}. \quad (4.15)$$

Our set of differential equations (4.9), (4.10) becomes

$$\frac{\partial \hat{T}}{\partial X} = -\frac{\partial^4 \hat{\psi}_1}{\partial \hat{y}^4}, \quad (4.16)$$

$$u_0 \frac{\partial \hat{T}}{\partial X} - u_0' \hat{y} \frac{\partial \hat{T}}{\partial \hat{y}} = \frac{\partial^2 \hat{T}}{\partial \hat{y}^2}, \quad (4.17)$$

with boundary conditions

$$\hat{T} = T_0(X), \quad \hat{\psi}_1 = \frac{\partial^2 \hat{\psi}_1}{\partial \hat{y}^2} = 0 \quad \text{on } \hat{y} = 0, \quad (4.18)$$

$$\hat{T} \rightarrow C, \quad \frac{\partial^2 \hat{\psi}_1}{\partial \hat{y}^2} \rightarrow -\omega_0(X) \quad \text{as } \hat{y} \rightarrow \infty. \quad (4.19)$$

The velocity adjustment therefore decouples from the temperature profile, and this allows us to make further analytical progress.

4.3. Analysis of the boundary layer problem

Integrating (4.16) twice with respect to \hat{y} gives

$$\frac{\partial^2 \hat{\psi}_1}{\partial \hat{y}^2} = -\omega_0(X) - \int_{\hat{y}}^{\infty} (s - \hat{y}) \frac{\partial \hat{T}(X, s)}{\partial X} ds, \quad (4.20)$$

where we have used (4.19). Now applying (4.18), we deduce from (4.17) and (4.20) that

$$\begin{aligned} \omega_0(X) &= - \int_0^{\infty} \hat{y} \frac{\partial \hat{T}(X, \hat{y})}{\partial X} d\hat{y} \\ &= \frac{C - T_0(X)}{u_0(X)} + \frac{2u_0'(X)}{u_0(X)} \int_0^{\infty} (C - \hat{T}(X, \hat{y})) \hat{y} d\hat{y}. \end{aligned} \quad (4.21)$$

In (4.21), $\hat{T}(X, \hat{y})$ is still unknown, but we can express the integral on the right-hand side in terms of C and $u_0(X)$ by considering the function $I_1(X)$ defined by

$$I_1(X) = \int_0^{\infty} (\hat{T}(X, \hat{y}) - C) \hat{y} d\hat{y}. \quad (4.22)$$

Now, using (4.17),

$$\begin{aligned}
 \frac{dI_1}{dX} &= \int_0^\infty \frac{\partial \hat{T}(X, \hat{y})}{\partial X} \hat{y} d\hat{y} \\
 &= \frac{u'_0}{u_0} \int_0^\infty \hat{y}^2 \frac{\partial \hat{T}}{\partial \hat{y}} d\hat{y} + \frac{1}{u_0} \int_0^\infty \hat{y} \frac{\partial^2 \hat{T}}{\partial \hat{y}^2} d\hat{y} \\
 &= -\frac{2u'_0}{u_0} \int_0^\infty \hat{y}(\hat{T} - C) d\hat{y} + \frac{C - T_0(X)}{u_0} \\
 &= -\frac{2u'_0}{u_0} I_1(X) + \frac{C - T_0(X)}{u_0}.
 \end{aligned} \tag{4.23}$$

It follows that

$$\frac{d}{dX} (u_0^2 I_1(X)) = u_0 (C - T_0(X)), \tag{4.24}$$

and hence

$$I_1(X) = -\frac{1}{u_0^2(X)} \int_X^1 u_0(s) (C - T_0(s)) ds, \tag{4.25}$$

which means that we can rewrite (4.21) as

$$\omega_0(X) = \frac{C - T_0(X)}{u_0(X)} + \frac{2u'_0(X)}{u_0^3(X)} \int_X^1 (C - T_0(s)) u_0(s) ds. \tag{4.26}$$

Recalling that the surface vorticity ω_0 is in principle a known linear functional of u_0 , we see that (4.26) is an integro-differential equation for $u_0(X)$. Indeed, if we use lubrication theory to approximate ω_0 by (4.8), then (4.26) can be transformed into the second-order nonlinear ordinary differential equation

$$u_0'' = \frac{u'_0 (T'_0 + 16u_0 u'_0)}{T_0 - C + 4u_0^2}, \tag{4.27}$$

where $' = d/dX$ and $T_0(X)$ is given but the core temperature C is still to be determined. We therefore expect to impose three conditions on (4.27). Since the fluid flows from the hot end of the bath ($X=1$) to the cold end of the bath ($X=0$), the upstream boundary condition is

$$u_0(1) = 0. \tag{4.28}$$

One other boundary condition comes from the global energy identity (2.14), that is

$$\int_0^1 \frac{\partial \hat{T}}{\partial \hat{y}}(X, 0) dX = 0. \tag{4.29}$$

We might guess that $u_0(0)$ should also be set to zero, but it can be shown that this is incompatible with (4.28) and (4.29) when T_0 is monotonic, and we will wait until § 5 to propose the final selection criterion.

We can transform (4.29) into a condition depending only on u_0 by solving (4.17) for \hat{T} as follows. If we introduce

$$\xi = -\int_X^1 u_0(s) ds, \quad \eta = -u_0(X)\hat{y}, \tag{4.30a, b}$$

then (4.17) is transformed into the heat equation

$$\frac{\partial \hat{T}}{\partial \xi} = \frac{\partial^2 \hat{T}}{\partial \eta^2}. \quad (4.31)$$

The boundary conditions are

$$\hat{T}(X(\xi), 0) = T_0(X(\xi)), \quad \hat{T}(X(\xi), \infty) = C, \quad (4.32)$$

where $X(\xi)$ follows from inverting (4.30a). Hence

$$\hat{T} = C - \frac{\eta}{2\sqrt{\cdot}} \int_0^\xi \frac{(C - T_0(X(s))) e^{-\eta^2/(4(\xi-s))}}{(\xi-s)^{3/2}} ds, \quad (4.33)$$

and (4.29) therefore reduces to

$$\begin{aligned} 0 &= \frac{1}{\sqrt{\cdot}} \int_0^1 \frac{(C - T_0(t)) u_0(t)}{\sqrt{-\int_0^t u_0(s) ds}} dt \\ &= -\frac{2}{\sqrt{\cdot}} \left((C-1) \sqrt{-\int_0^1 u_0(t) dt} + \int_0^1 T_0'(t) \sqrt{-\int_0^t u_0(s) ds} dt \right). \end{aligned} \quad (4.34)$$

Once we have solved for $u_0(X)$ from (4.27), (4.28), and (4.34), we can find the velocity perturbation in the boundary layer from (4.20) as

$$\hat{u}_1 = \frac{\partial \hat{\psi}_1}{\partial \hat{y}} = -4\hat{y}u_0(X) + \frac{\partial I_2}{\partial X}, \quad (4.35)$$

where I_2 is defined as

$$I_2(X, \hat{y}) := \frac{1}{2} \int_{\hat{y}}^\infty (s - \hat{y})^2 (T(X, s) - C) ds. \quad (4.36)$$

After a few manipulations we find

$$I_2(X, \hat{y}) = \frac{1}{u_0^3(X)} \int_0^\xi (C - T_0(X(s))) \left(\frac{2}{\sqrt{\cdot}} \sqrt{\xi-s} e^{-\eta^2/4(\xi-s)} - \eta \operatorname{erfc} \left(\frac{\eta}{2\sqrt{\xi-s}} \right) \right) ds. \quad (4.37)$$

4.4. Solution procedure

From now on we concentrate on the case where $T_0(X) = X$. Let us suppose for the moment that C is given. Then our task is to solve

$$u_0'' = \frac{u_0'(1 + 16u_0u_0')}{X - C + 4u_0^2}, \quad (4.38)$$

subject to $u_0(1) = 0$ and the flux condition (4.34). This can be viewed as a shooting problem: we solve (4.38) numerically starting from $X = 1$ and vary $u_0'(1)$ as a shooting parameter until (4.34) is satisfied.

This procedure can be implemented by noting that, for any λ , (4.38) is invariant under the transformation

$$u_0 = \frac{\bar{u}_0}{\sqrt{1-\lambda}}, \quad X = 1 - \frac{1-\bar{X}}{1-\lambda}, \quad C = \frac{\bar{C}-\lambda}{1-\lambda}. \quad (4.39)$$

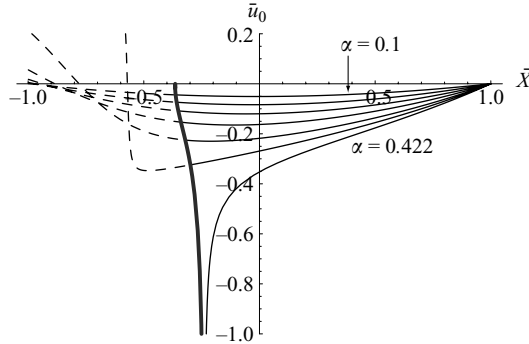


FIGURE 7. Horizontal velocity \bar{u}_0 plotted as a function of \bar{X} with $\bar{u}'_0(1) = \alpha = 0.1, 0.16, 0.22, 0.28, 0.34, 0.38, 0.422$. The thicker line represents the points $(\bar{X}, \bar{u}_0(\bar{X}))$ for which (4.41) is satisfied.

Our approach, then, is to set $\bar{C} = 0$ and solve

$$\bar{u}''_0 = \frac{\bar{u}'_0 (1 + 16\bar{u}_0\bar{u}'_0)}{\bar{X} + 4\bar{u}_0^2}, \quad (4.40)$$

where now $' = d/d\bar{X}$, subject to $\bar{u}_0(1) = 0, \bar{u}'_0(1) = \alpha$. For each choice of α , we determine the value of λ (if it exists) such that (4.34) is satisfied, i.e.

$$\sqrt{-\int_{\lambda}^1 \bar{u}_0(t) dt} = \int_{\lambda}^1 \sqrt{-\int_{\lambda}^t \bar{u}_0(s) ds} dt. \quad (4.41)$$

Each such solution $\bar{u}_0(\bar{X})$ corresponds, via the transformation (4.39), to a solution $u_0(X)$ of the original problem, with $C = -\lambda/(1-\lambda)$.

The results of this procedure are shown in figure 7, where the line on which (4.41) is satisfied is shown as the thick curve. We see that $\lambda < 0$ is an increasing function of α , with $\lambda \rightarrow -0.364$ as $\alpha \rightarrow 0$. This corresponds to a value of $C \approx 0.267$. Moreover, figure 7 reveals that there is a critical value for α , say α^* , such that if $\alpha < \alpha^*$, $\bar{u}(\bar{X}) \rightarrow -\infty$ before the condition (4.41) is satisfied. This critical value is approximately equal to 0.422, which corresponds to $\lambda \simeq -0.238, C = C_{\min} \simeq 0.192$. At $C = C_{\min}$,

$$\bar{u} \sim (\bar{X} - \lambda)^{-1/3}, \quad (4.42)$$

as $\bar{X} \rightarrow \lambda$.

In summary, it is only for values of C in the interval $C \in (0.192, 0.267)$, that there is a solution for u_0 of (4.27) satisfying (4.28) and (4.29). This is certainly in the same range as values of C predicted by our numerical solutions in §3. However, we still need some further mechanism to select a specific value of C from our boundary layer model.

5. The selection of the core temperature

One possible procedure for selecting C would be to consider the fate of the boundary layer after it has impacted the corner $X = 0, y = 1$. The numerical evidence of figures 2–4 suggests that it transforms itself into a vertical layer which may ultimately transmit information about the value of C all the way round the boundary of the tank to the corner $X = y = 1$.

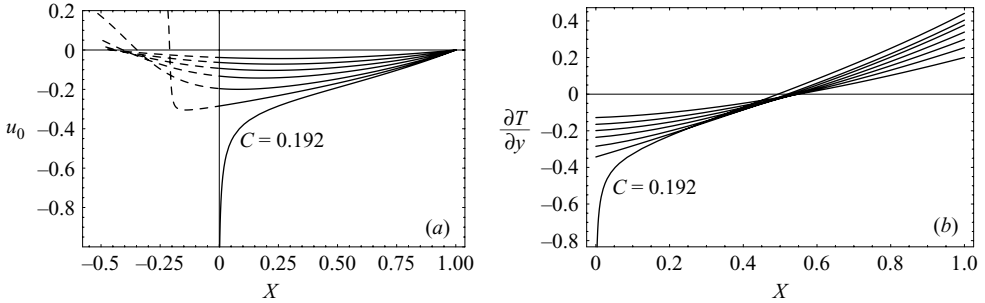


FIGURE 8. (a) Horizontal velocity u_0 and (b) $\partial T / \partial \hat{y}|_{\hat{y}=0}$ plotted as functions of X with $C = 0.266, 0.264, 0.260, 0.253, 0.243, 0.230, 0.192$.

However, in the hope that C can be found just from consideration of the boundary layer near $y = 1$, we have plotted $u_0(X)$ and $\partial T / \partial y|_{y=1}$ for several admissible values of C in figure 8. We see that $C = 0.192 \dots$ is distinctive in being the value for which

$$\lim_{X \downarrow 0} \frac{\partial T}{\partial y}(X, 1) = -\infty, \quad (5.1)$$

i.e. it gives the greatest vertical temperature gradient in the corner. It is conceivable that the boundary layer needs to encounter such a temperature gradient for it to be sufficiently unstable to give birth to a downward flowing layer near $X = 0$. We also notice from figure 8(a) that this smallest value of C gives the maximum value of u_0^2 for any X and hence the maximum dissipation rate. In addition, figure 5 is suggestive of a surface velocity that begins bending towards minus infinity before levelling off in a narrow region near $X = 0$. This numerical evidence is our first hint that C takes its minimum possible value C_{\min} .

To provide analytical justification for this seemingly arbitrary choice of C , we now briefly examine the fate of the thermal boundary layer as it turns the corner and descends the cold left-hand wall of the bath. We are handicapped by the fact that this boundary layer has to match with a fully two-dimensional Stokes flow region in which $X = O(\delta)$ and analytical solution appears to be impossible. Nevertheless, we can infer from our outer solution that the surface velocity in this Stokes flow region is $O(1)$ unless $C = C_{\min}$, in which case (4.42) implies that it is much larger, of order $\delta^{-1/3}$.

We proceed as follows. First we make the assumption that the temperature is, to leading order, convected through the corner region. Since $\psi = O(\varepsilon)$ in the thermal boundary layer on the top surface, this implies that ψ is also $O(\varepsilon)$ in the cold wall boundary layer in which $O(1)$ variations in T occur. We then obtain a dominant balance in the governing equations (2.9)–(2.10) via the rescalings

$$x = \varepsilon \delta^{1/3} \tilde{x}, \quad \psi = \varepsilon \tilde{\psi}. \quad (5.2)$$

Neglecting terms of order ε^2 , we thus obtain the equations

$$\frac{\partial T}{\partial \tilde{x}} = \frac{\partial^4 \tilde{\psi}}{\partial \tilde{x}^4}, \quad \frac{\partial \tilde{\psi}}{\partial y} \frac{\partial T}{\partial \tilde{x}} - \frac{\partial \tilde{\psi}}{\partial \tilde{x}} \frac{\partial T}{\partial y} = \delta^{2/3} \frac{\partial^2 T}{\partial \tilde{x}^2} \quad (5.3)$$

in this boundary layer.

To leading order in δ , T is convected with the flow, so we can write $T = F(\tilde{\psi})$, where F is determined in principle by inlet conditions from the corner problem. Matching

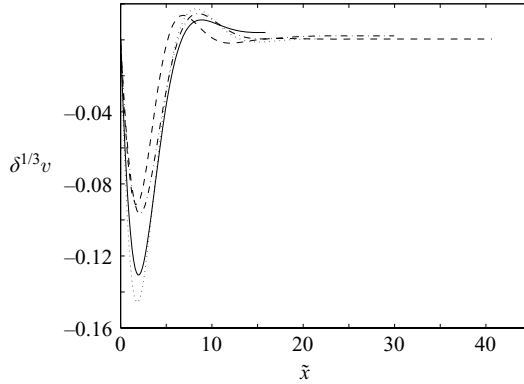


FIGURE 9. Vertical velocity scaled with $\delta^{1/3}$ on $y=0.5$ as a function of $\tilde{x}=x/\delta^{1/3}\varepsilon$ for (0.1, 0.25) (solid curve), $(\varepsilon, \delta)=(0.053, 0.25)$ (dashed-dotted curve), (0.1, 0.1) (dotted curve), and (0.1, 0.053) (dashed curve).

with a constant temperature C in the core flow, we thus obtain

$$\frac{\partial^3 \tilde{\psi}}{\partial \tilde{x}^3} = F(\tilde{\psi}) - C, \quad (5.4)$$

subject to the boundary conditions

$$\tilde{\psi} = \frac{\partial \tilde{\psi}}{\partial \tilde{x}} = 0 \quad \text{at} \quad \tilde{x} = 0, \quad (5.5)$$

$$\frac{\partial^2 \tilde{\psi}}{\partial \tilde{x}^2} \rightarrow 0 \quad \text{as} \quad \tilde{x} \rightarrow \infty. \quad (5.6)$$

Although we cannot solve this problem without knowledge of the function $F(\tilde{\psi})$, we can deduce that $\tilde{\psi}$ and T must both be independent of y in this region. It follows that there is a constant vertical velocity \tilde{v} such that

$$\frac{\partial \tilde{\psi}}{\partial \tilde{x}} \rightarrow \tilde{v} \quad \text{as} \quad \tilde{x} \rightarrow \infty, \quad (5.7)$$

and the leading-order matching condition for the outer two-dimensional Stokes flow is thus

$$\frac{\partial \psi}{\partial x} = \delta^{-1/3} \tilde{v} \quad \text{on} \quad x = 0. \quad (5.8)$$

The presence of the $\delta^{-1/3}$ term in (5.8) means that the surface velocity feeding into the corner region in the upper left-hand corner of the bath is of the same order as the descent velocity if and only if $C = C_{\min}$. Moreover, this choice minimizes the singularity experienced by the outer Stokes flow in the corner. Numerical evidence that the scaling (5.2) in the cold wall boundary layer is correct is provided by figure 9, where we have plotted the scaled vertical velocity as a function of the scaled coordinate $\tilde{x} = \delta^{-1/3} \varepsilon^{-1} x$.

We remark that there is a further inner region closer still to the cold wall in which the fluid velocity tends to zero and thermal diffusion regains its importance. In this region, the flow is given by

$$\tilde{\psi} \sim \frac{\alpha \tilde{x}^2}{2}, \quad (5.9)$$

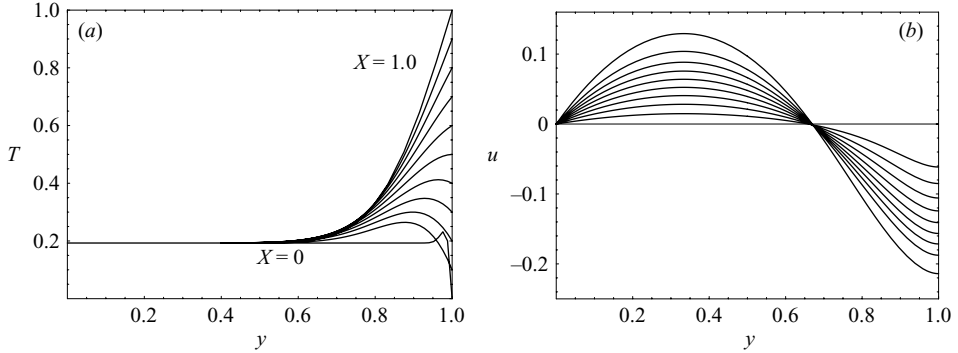


FIGURE 10. Plot of the asymptotic solution for the temperature (a) and the velocity (b) as a function of y for $X = 0.0, 0.1, \dots, 1.0$ with $C = 0.1928$ and $\varepsilon = 0.1$.

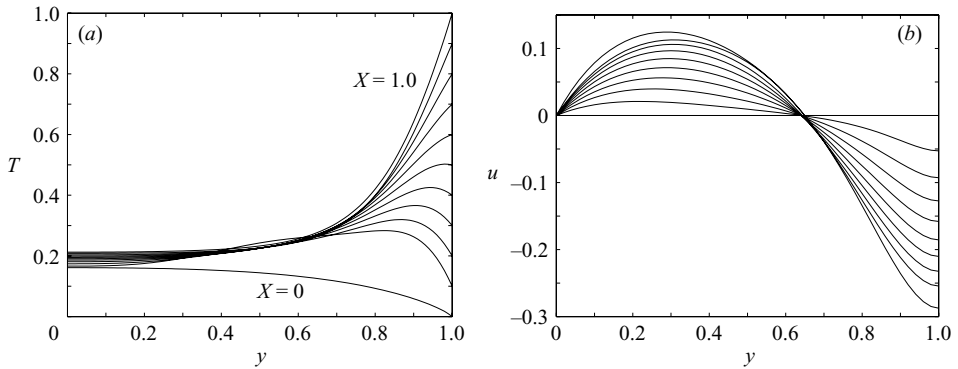


FIGURE 11. Plot of the numerical solution for temperature (a) and the velocity (b) as a function of y for $X = 0, 0.1, \dots, 1.0$ with $\delta = 0.25$ and $\varepsilon = 0.1$ (or $Ra = 1.6 \times 10^5$).

where $\alpha = d^2\tilde{\psi}/d\tilde{x}^2(0)$, and the rescaling $\tilde{x} = \delta^{2/9}\tilde{\xi}$ yields the equation

$$-\alpha\tilde{x} \frac{\partial T}{\partial y} = \frac{\partial^2 T}{\partial \tilde{\xi}^2} \quad (5.10)$$

for $T(y, \tilde{\xi})$. This equation governs the y -variations in T near the left-hand wall observed in figures 2–4.

6. Discussion

It is now important to compare our asymptotic solution for $C = C_{\min}$ with the two-dimensional numerical solutions when $T_0 = X$. We choose $\varepsilon = 0.1$, corresponding to $Ra = 1.6 \times 10^5$ when $\delta = 0.25$ or $Ra = 10^6$ when $\delta = 0.1$. In figure 10 we plot, as a function of $y = 1 - \varepsilon\hat{y}$, the composite asymptotic approximations for the temperature T and the velocity u given respectively by

$$T \sim \hat{T}, \quad u \sim u_0(X)y(3y - 2) + \varepsilon\hat{u}_1, \quad (6.1)$$

where \hat{T} is given by (4.33) and u_0 and \hat{u}_1 follow from (4.27) and (4.35). In figures 11 and 12 we plot the corresponding numerical solutions with $\delta = 0.25$ and $Ra = 1.6 \times 10^5$, and $\delta = 0.1$ and $Ra = 10^6$, respectively. From these three figures, we observe that, for $X \geq 0.1$, the boundary layer solution and the numerical solution for the temperature

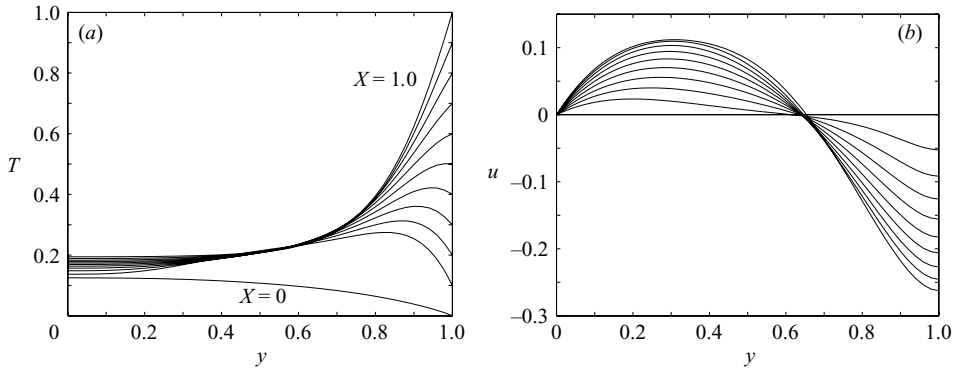


FIGURE 12. Plot of the numerical solution for the temperature (a) and the velocity (b) as a function of y for $X = 0, 0.1, \dots, 1.0$ with $\delta = 0.1$ and $\varepsilon = 0.1$ (or $Ra = 10^6$).

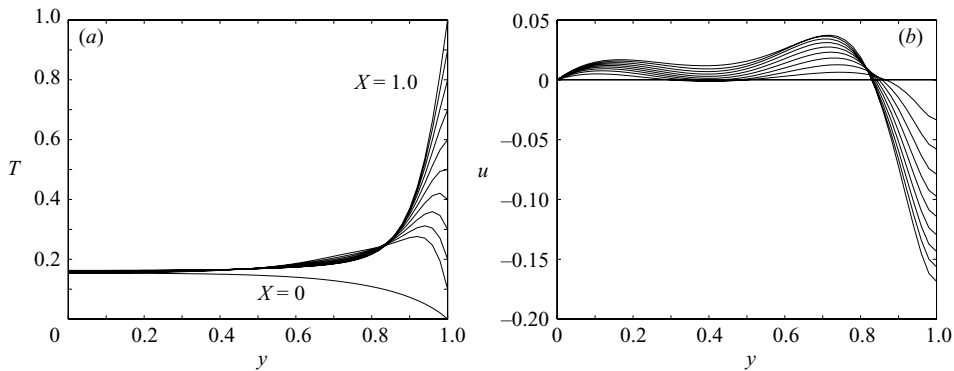


FIGURE 13. Plot of the numerical solution for the temperature (a) and the velocity (b) as a function of y for $X = 0, 0.1, \dots, 1.0$ with $\delta = 0.25$ and $\varepsilon = 0.035$ (or $Ra = 10^7$).

and the velocity are in good agreement with each other even for this relatively large value of ε . In particular, both the numerical solution and the asymptotic solution for the horizontal velocity are roughly parabolic in y in the core. However, if we increase the Rayleigh number to $Ra = 10^7$ in a bath with $\delta = 0.25$, Figure 13 reveals that the horizontal velocity profile in the numerical solution is no longer parabolic in the core. This prompts us to reconsider, for high Rayleigh numbers, the validity of our assumption that, away from boundary layers, there is a core flow of closed streamlines that occupies most of the bath.

The possibility that the core flow is disrupted by the fluid mechanics near the base $y = 0$ leads us to make a conjecture about the fate of the cold wall boundary layer when it emerges from the corner $X = 0, y = 0$. Figure 11(a) reveals that although there is a stable thermal stratification adjacent to the cold wall, the temperature to which the core flow has to match as $X \rightarrow 0$ can be unstably stratified for small y , and that the intensity of this unstable stratification increases as ε , and hence the mechanical boundary layer thickness, decreases. Moreover, we observe from figure 14 that, for sufficiently small values of ε , the cold wall boundary layer ceases to generate a gravity current along the lower wall but rather appears to separate from the base and penetrate the core as it emerges from the corner. This means that the core is no longer isothermal and explains the non-parabolic core velocity profiles of figure 13. Our asymptotic solution, obtained in the limit $\varepsilon \rightarrow 0$, therefore seems to fail if ε is

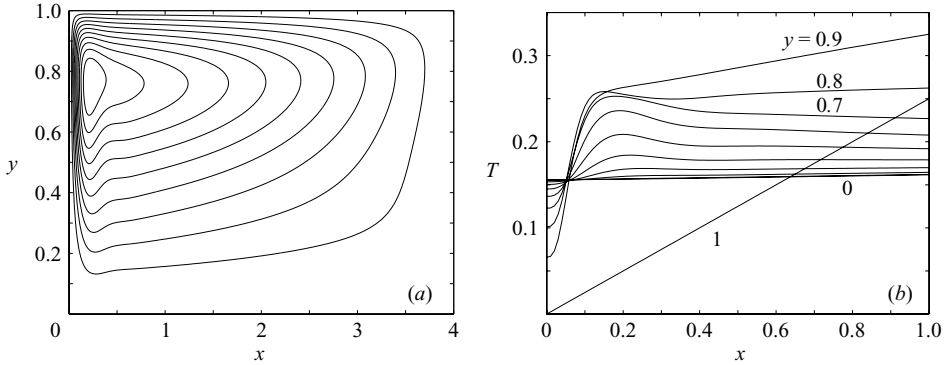


FIGURE 14. Plot of streamlines (a) and the temperature as a function of x for $y = 0, 0.1, \dots, 1$ (b) in the case where $\varepsilon = 0.053$ and $\delta = 0.25$ (or $Ra = 2 \times 10^6$).

too small! We hypothesize that our solution applies in an asymptotic regime of the form $f(\delta) \ll \varepsilon \ll 1$, although we have thus far been unable to identify the form of $f(\delta)$: there does not appear to be a straightforward criterion for separation of the boundary layer on $y = 0$.

In conclusion, we remark that our analysis would need to be changed radically had we imposed a no-slip boundary condition at $y = 1$. In such a situation, the scaling for U would have been

$$\frac{U}{\varepsilon^3 \delta \sqrt{Ra}} = 1, \quad \frac{1}{\varepsilon^2 Ra} \frac{1}{U} = 1, \quad (6.2)$$

instead of (4.14) and (4.15), leading to

$$U = (\delta^2 Ra)^{1/10}, \quad \varepsilon = (\delta^2 Ra)^{1/5}. \quad (6.3)$$

Moreover, the thermal and mechanical boundary layer would now be intimately coupled, making the mathematical analysis far less tractable.

7. Conclusion

In this paper, we have used numerical and analytical methods to analyse the convective flow induced by applying a horizontal thermal gradient to the surface of a viscous fluid. Our study was motivated by batch melting in a glass furnace, but we have concentrated on a paradigm problem that simplifies the physics and the geometry while retaining the features associated with the convective flow.

In the physically relevant limit of large Prandtl number and large Rayleigh number, we began by assuming that the flow was such that the temperature is approximately constant in the bulk of the fluid. The flow is therefore effectively a Stokes flow driven entirely by the boundary layers, in which the thermal gradients are significant. We have analysed the boundary layer at the top of the fluid when the upper surface is stress-free. In this case, the shear stress is zero to leading order throughout the boundary layer, which therefore becomes a vorticity layer. We find that the solution may be characterized by the surface velocity which in general satisfies an integro-differential equation. This may be reduced to a second-order ordinary differential equation if the bath is assumed to be long and thin so that lubrication approximation applies. Solutions of this equation give good agreement with our full numerical solutions, although one parameter, namely the temperature C in the bulk of the

fluid, remains undetermined. There are several possible reasons why the value of C that maximizes the thermal gradient at the downstream end of the boundary layer might be selected, but, to resolve the indeterminacy, we have needed to study the fate of the boundary layer as it encounters the left-hand wall of the bath. Although our analytical and numerical analysis of this ‘cold wall’ boundary layer gave us confidence in the selection mechanism for C , it also pointed to the fact that, for a given bath geometry, our asymptotic solution is not uniformly valid as the Rayleigh number tends to infinity. We have suggested that this is because the cold wall boundary layer cannot sustain a gravity current down the base of the bath when the bath aspect ratio is high enough; instead, it returns into the core flow, thereby invalidating our assumption that the core is isothermal.

In a real glass furnace, many other effects that we have ignored may be important. We also recall that the variation of viscosity with temperature and radiative heat transfer are both likely to be very significant. We note, though, that when the temperature is roughly constant in the core such effects may be confined to the boundary layers that we have analysed. This also helps to justify our neglect of heat transfer through the walls of the bath. Finally, we point out that three-dimensional flows are often observed in practice.

The authors would like to thank Dr A. C. Fowler, Dr G. Kozyreff, Prof. J. R. Lister, Prof. E. J. Hinch and Mr S. Chiu-Webster for helpful comments and suggestions and Dr. U. Lange of Schott for drawing the problem to their attention. Also, §6 was written as the result of the perspicacious comments of two referees. This paper has been supported by the project MAGICAL (<http://www.win.tue.nl/ccee/MAGICAL/>).

Note added in proof After this paper had been accepted for publication the authors became aware of work by Chiu-Webster, Hinch & Lister (2007) in which the top boundary layer thickness is argued to be of $O(Ra^{-1/5})$.

REFERENCES

- BATCHELOR, G. K. 1954 Heat transfer by free convection across a closed cavity between vertical boundaries at different temperatures. *Q. Appl. Maths.* **12**, 209–233.
- BATCHELOR, G. K. 1956 On steady laminar flow with closed streamlines at large Reynolds number. *J. Fluid Mech.* **1**, 177–190.
- CHIU-WEBSTER, S., HINCH, E. J. & LISTER, J. R. 2007 Very viscous horizontal convection. *J. Fluid Mech.* (submitted).
- CORMACK, D. E., LEAL, L. G. & IMBERGER, J. 1974 Natural convection in a shallow cavity with differentially heated end walls. Part 1. Asymptotic theory. *J. Fluid Mech.* **65**, 209–229.
- DANIELS, P. G. 1993 High Rayleigh number thermal convection in a shallow laterally heated cavity. *Proc. R. Soc. Lond. A* **440**, 274–289.
- ELDER, J. W. 1965 Laminar free convection in a vertical slot. *J. Fluid Mech.* **23**, 77–98.
- GILL, Á. E. 1966 The boundary-layer regime for convection in a rectangular cavity. *J. Fluid Mech.* **26**, 515–536.
- KRAUSE, D. & LOCH, H. 2002 *Mathematical Simulation in Glass Technology*. Springer.